

Microscopic analysis of the characteristic energy loss spectra for fast electrons in 4d-metals

I. I. Mazin, E. G. Maksimov, S. N. Rashkeev, and Yu. A. Uspenskii

P. N. Lebedev Physics Institute, Academy of Sciences of the USSR

(Submitted 2 August 1985)

Zh. Eksp. Teor. Fiz. **90**, 1092–1110 (March 1986)

The properties of the characteristic energy loss spectra for fast electrons in 4d-metals are discussed, and formulas are derived for calculating the loss spectra by the density functional method. Numerical calculations for the 4d-metals give results in good qualitative and quantitative agreement with experiment. The nonuniform energy distribution of the electron states above the Fermi level and, particularly, the deep trough in the state density $N(E)$ between the d - and the p -bands, are primarily responsible for the distinctive features of the loss spectra in the transition metals. These features depend on the relative position and width of the d -, p -, and f -bands and the extent to which they are filled, i.e., on the atomic number of the metal and its atomic volume. The crystal structure merely determines the fine structure of the frequency dependence of the loss spectrum and is of secondary importance.

INTRODUCTION

The characteristic energy loss spectra for fast electrons passing through thin films or reflected at the surface have been under active experimental study ever since the 1950s, and a great deal of knowledge has been gained regarding the loss spectra in metals, semiconductors, and dielectrics.^{1,2} It was discovered quite early that there is a wide class of materials (simple metals and semiconductors with s - p valence electrons) whose characteristic energy loss spectra exhibit a strong plasma resonance which corresponds to the excitation of collective oscillations in the conduction electron density. For zero momentum transfer $\mathbf{q} = 0$, the plasma resonance frequency is almost identical to the frequency $\omega_p = (4\pi ne^2/m)^{1/2}$ for classical plasma oscillations in a homogeneous electron gas (here n is the electron density). The plasma resonance frequency shifts as the momentum \mathbf{q} varies; these shifts characterize the spectrum of the collective excitations of the electron density in the crystal and also agree quite closely with the values calculated for a homogeneous electron gas. Perturbation theory based on expansions in the weak electron-ion pseudopotential accurately describes the small discrepancies in the plasma oscillation spectra for simple metals as compared with the homogeneous electron gas model (we refer the reader to Sturm's review³).

However, there are many materials (e.g., the transition and noble metals) whose characteristic energy loss spectra differ from the predictions of the homogeneous electron gas model. In this case the loss spectra typically contain several peaks, which are frequently quite broad and unsymmetric. D. Pines⁴ observed 20 years ago that this behavior is due to the strength of the electron-ion interaction in the transition metals, which greatly distorts the electron structure (as compared with the case of nearly free electrons) in a wide energy interval $\Delta E \sim \hbar\omega_p$ near the Fermi surface.

The last three decades have seen great advances in experimental techniques for analyzing the characteristic ener-

gy loss spectra. In particular, synchrotron radiation can be used to analyze the collective oscillations in the electron gas in metals at energies $\hbar\omega_p \lesssim 40$ eV by means of purely optical techniques. Although less progress has been made in the theoretical domain, our understanding has improved regarding the dielectric permittivity of the electron gas, which determines the loss spectra. So far, only empirical models have been proposed to describe the loss spectra for the transition metals, and these models suffer from a lack of reliable data on the electron structure for these metals. The properties of the characteristic energy loss spectra for the transition metals thus remain unclear.

Recent improvements in methods for calculating the electron structure have made it possible to calculate the optical properties of metals *ab initio*. Several such calculations were carried out in Refs. 5 and 6. We use this method here to calculate the loss spectra for zero momentum transfer $\mathbf{q} = 0$. The calculations were carried out for all eight of the 4d-transition metals from yttrium to palladium, and the results are in close agreement with experimental data. We are thus able to analyze the characteristic energy loss spectra for the transition metals in detail and to identify the factors that affect the losses. This analysis constitutes the principal goal of this paper, which is organized as follows. In Sec. 1 we derive formulas for calculating the loss spectrum by the density functional technique and present the fundamental results for the permittivity of metals. In Sec. 2 we briefly describe the computational procedure and its accuracy, discuss the basic properties of the electron structure in the 4d-metals, and compare the calculated loss spectra with experimental data. Section 3 is devoted to an analysis of the primary factors responsible for determining the loss spectrum in the 4d-transition metals, and the dependence of the spectrum on the crystal and electron structure of the metal is discussed. The paper closes with a brief summary of the main results, and suggestions are given for extending them to a wider class of materials.

I. CALCULATION OF THE LOSS SPECTRUM BY THE DENSITY FUNCTIONAL TECHNIQUE

In the Born approximation, energy and momentum transfer from a fast electron to the electrons in a metal is described by the differential scattering cross section

$$\frac{d^2\sigma}{d\varepsilon_k, d\Omega_k} = \frac{k_1}{k_0} \left(\frac{e^2}{\varepsilon_q} \right) S(\mathbf{q}, \omega). \quad (1)$$

Here $\hbar\mathbf{k}_0$ and $\hbar\mathbf{k}_1$ are the momenta of the fast electron before and after scattering, $\varepsilon_q = \hbar^2 q^2 / 2m$, ε_{k_1} is the electron energy after scattering, and $\hbar\omega = \varepsilon_{k_0} - \varepsilon_{k_1}$. The dynamic structure factor $S(\mathbf{q}, \omega)$ is directly related to the macroscopic permittivity $\varepsilon_m(\mathbf{q}, \omega)$ by

$$S(\mathbf{q}, \omega) = \frac{1}{\pi V(\mathbf{q})} \text{Im} \left(- \frac{1}{\varepsilon_m(\mathbf{q}, \omega)} \right), \quad (2)$$

where $V(\mathbf{q}) = 4\pi e^2 / q^2$.

The permittivity is one of the most important characteristics of the electron gas in metals, because it not only determines the spectrum of the collective electron density oscillations but also yields information regarding one-electron excitations. The transverse permittivity $\varepsilon_{tr}(\mathbf{q}, \omega)$ with $\mathbf{q} = 0$ determines the optical properties of the metal.¹⁾ When $\mathbf{q} = 0$, the loss spectrum can be found experimentally by letting a beam of fast electrons pass through thin films. On the other hand, the momentum transfer is not determined in experiments in which fast electrons are reflected by a surface—in this case, the recorded dependence of the characteristic energy losses on ω represents an average over a wide interval of momentum transfers. Since the permittivity determines the loss spectrum almost completely for fast electrons, we will discuss it more fully.

The dielectric response functions of crystals are described by matrices⁷ in terms of vectors \mathbf{G} and \mathbf{G}' in reciprocal lattice space. The macroscopic permittivity $\varepsilon_m(\mathbf{q}, \omega)$ can be expressed in terms of the diagonal matrix element for the inverse permittivity $\varepsilon^{-1}(\mathbf{q} + \mathbf{G}, \mathbf{q} + \mathbf{G}', \omega)$ with $\mathbf{G} = \mathbf{G}' = 0$:

$$\varepsilon_m(\mathbf{q}, \omega) = [\varepsilon^{-1}(\mathbf{q} + \mathbf{0}, \mathbf{q} + \mathbf{0}, \omega)]^{-1}. \quad (3)$$

In turn, we can express ε^{-1} in terms of the susceptibility matrix $\chi(\mathbf{q} + \mathbf{G}, \mathbf{q} + \mathbf{G}', \omega)$ for the electrons:

$$\varepsilon^{-1}(\mathbf{q} + \mathbf{G}, \mathbf{q} + \mathbf{G}', \omega) = \delta_{\mathbf{G}\mathbf{G}'} + \frac{4\pi e^2}{|\mathbf{q} + \mathbf{G}|^2} \chi(\mathbf{q} + \mathbf{G}, \mathbf{q} + \mathbf{G}', \omega). \quad (4)$$

We need to calculate ε from data on the band structure of the metal. Since most modern band structure calculations (including ours) employ the density functional technique^{8,9} (see also the reviews in Refs. 10, 11), it is important to have an expression for χ which is derived using this technique.

The density functional technique reduces the many-body problem to solving the Schrödinger equation for a single particle with a self-consistent potential $V_{\text{eff}}(\mathbf{r})$:

$$\left(- \frac{\hbar^2 \nabla^2}{2m} + V_{\text{eff}}(\mathbf{r}) \right) \psi_{\mathbf{k}\lambda}(\mathbf{r}) = E_{\mathbf{k}\lambda} \psi_{\mathbf{k}\lambda}(\mathbf{r}). \quad (5)$$

The potential $V_{\text{eff}}(\mathbf{r})$ depends explicitly only on the external

field potential $V_{\text{ext}}(\mathbf{r})$ (the ion potential for a crystal) and on the electron density $n(\mathbf{r})$,

$$V_{\text{eff}}(\mathbf{r}) = V_{\text{ext}}(\mathbf{r}) + V_H(\mathbf{r}) + V_{xc}(\mathbf{r}), \quad (6)$$

where $n(\mathbf{r})$ is expressible in terms of the eigenfunctions of Eq. (5):

$$n(\mathbf{r}) = \sum_{\mathbf{k}\lambda} f_{\mathbf{k}\lambda} |\psi_{\mathbf{k}\lambda}(\mathbf{r})|^2. \quad (7)$$

Here $f_{\mathbf{k}\lambda}$ is the electron distribution function,

$$V_H(\mathbf{r}) = e^2 \int d\mathbf{r}' n(\mathbf{r}') / |\mathbf{r} - \mathbf{r}'|$$

is the Hartree potential, and $V_{xc} = \delta E_{xc} / \delta n(\mathbf{r})$ is the exchange-correlation potential. The "local" approximation is generally used to derive explicit expressions for the exchange-correlation energy E_{xc} and potential $V_{xc}(\mathbf{r})$. Since space is limited, we will not discuss all the problems involved in calculating these quantities, for which we refer to Ref. 10. However, we will sketch how χ can be calculated in this approach; the static case^{11,12} will be considered first.

A small perturbation $\delta V_{\text{ext}}(\mathbf{r})$ in the external field produces a change $\delta n(\mathbf{r})$ in the electron density, and the effective potential is also altered:

$$\delta V_{\text{eff}}(\mathbf{r}) = \delta V_{\text{ext}}(\mathbf{r}) + e^2 \int \frac{\delta n(\mathbf{r}')}{|\mathbf{r} - \mathbf{r}'|} d\mathbf{r}' + \int \frac{\delta V_{xc}(\mathbf{r}')}{\delta n(\mathbf{r}')} \delta n(\mathbf{r}') d\mathbf{r}', \quad (8)$$

Solving (5) to first order in δV_{eff} , we find the change $\delta \psi_{\mathbf{k}\lambda}(\mathbf{r})$ is the wave function and then use (7) to get the final result

$$\delta n(\mathbf{r}) = \int \chi_0(\mathbf{r}, \mathbf{r}') \delta V_{\text{eff}}(\mathbf{r}') d\mathbf{r}', \quad (9)$$

where $\chi_0(\mathbf{r}, \mathbf{r}')$ is the static susceptibility for a system of non-interacting electrons described by the Schrödinger equation (5). We now solve Eqs. (8) and (9) simultaneously and recall the definition

$$\delta n(\mathbf{r}) = \int \chi(\mathbf{r}, \mathbf{r}') \delta V_{\text{ext}}(\mathbf{r}') d\mathbf{r}' \quad (10)$$

of the total electron susceptibility; the formally exact expression

$$\begin{aligned} \chi^{-1}(\mathbf{q} + \mathbf{G}, \mathbf{q} + \mathbf{G}', 0) \\ = \chi_0^{-1}(\mathbf{q} + \mathbf{G}, \mathbf{q} + \mathbf{G}', 0) - \frac{4\pi e^2}{|\mathbf{q} + \mathbf{G}|^2} \delta_{\mathbf{G}\mathbf{G}'} - \frac{\delta V_{xc}(\mathbf{q} + \mathbf{G})}{\delta n(\mathbf{q} + \mathbf{G}')} \end{aligned} \quad (11)$$

for the static susceptibility matrix then follows without difficulty.

The dynamic response functions at frequencies $\sim \omega_p$ —not the static response functions—are needed to analyze the characteristic energy loss spectrum. Strictly speaking, the density functional method in its existing form is not adequate for this purpose. However, a simple generalization of this method has been suggested in Refs. 13 and 14 for calculating the dynamic linear response functions. One assumes

that Eqs. (6) and (8) remain valid when a weak, time-dependent perturbation $\delta V_{\text{ext}}(\mathbf{r}, t)$ is applied, and that the functional dependence of $V_{\text{xc}}(\mathbf{r}, t)$ on the density $n(\mathbf{r}, t)$ remains the same as in the static case. Retracing the steps used to derive (7)–(11), we then readily obtain

$$\chi^{-1}(\mathbf{q}+\mathbf{G}, \mathbf{q}+\mathbf{G}', \omega) = \chi_0^{-1}(\mathbf{q}+\mathbf{G}, \mathbf{q}+\mathbf{G}', \omega) - \frac{4\pi e^2}{|\mathbf{q}+\mathbf{G}|^2} \delta_{\mathbf{G}\mathbf{G}'} \frac{\delta V_{\text{xc}}(\mathbf{q}+\mathbf{G}, \omega)}{\delta n(\mathbf{q}+\mathbf{G}', \omega)}. \quad (12)$$

The dynamic susceptibility χ_0 in (11) for noninteracting electrons is given by

$$\chi_0(\mathbf{q}+\mathbf{G}, \mathbf{q}+\mathbf{G}', \omega) = \frac{2}{\Omega} \sum_{\mathbf{k}, \lambda, \lambda'} \frac{f_{\mathbf{k}+\mathbf{q}, \lambda'} - f_{\mathbf{k}\lambda}}{\hbar\omega - E_{\mathbf{k}+\mathbf{q}, \lambda'} + E_{\mathbf{k}\lambda} + i\delta} \times \langle \mathbf{k}\lambda | e^{-i(\mathbf{q}+\mathbf{G}')\cdot\mathbf{r}} | \mathbf{k}+\mathbf{q}, \lambda' \rangle \langle \mathbf{k}+\mathbf{q}, \lambda' | e^{i(\mathbf{q}+\mathbf{G})\cdot\mathbf{r}} | \mathbf{k}\lambda \rangle, \quad (13)$$

where $|\mathbf{k}\lambda\rangle$ is the Bloch wave function for an electron in band λ with wave vector \mathbf{k} and energy $E_{\mathbf{k}\lambda}$.

Equation (12) implies that the dynamic susceptibility calculated under the above assumptions merges smoothly with the exact static susceptibility as $\omega \rightarrow 0$, which suggests that Eq. (11) describes $\chi(\mathbf{q}+\mathbf{G}, \mathbf{q}+\mathbf{G}', \omega)$ quite accurately at low frequencies. The corrections are expected to be significant only for relatively high frequencies. Moreover, the eigenfunctions $|\mathbf{k}\lambda\rangle$ and energies $E_{\mathbf{k}\lambda}$ in (13) may be assumed to coincide to high accuracy with the corresponding eigenfunctions and energies for the one-particle equation (5) (Ref. 15).

With the above qualifications, Eqs. (12) and (13) make it possible to calculate the electron susceptibility by using data from band-structure calculations. However, in practice this approach is difficult because the matrices in Eq. (12) are inverted. To understand the physics underlying this procedure, we introduce two additional matrices $\tilde{\chi}$ and $\tilde{\chi}$ defined by

$$\varepsilon(\mathbf{q}+\mathbf{G}, \mathbf{q}+\mathbf{G}', \omega) = \delta_{\mathbf{G}\mathbf{G}'} - \frac{4\pi e^2}{|\mathbf{q}+\mathbf{G}|^2} \tilde{\chi}(\mathbf{q}+\mathbf{G}, \mathbf{q}+\mathbf{G}', \omega), \quad (14)$$

$$\varepsilon_{\text{ex}}(\mathbf{q}, \omega) = 1 - \frac{4\pi e^2}{q^2} \tilde{\chi}(\mathbf{q}+\mathbf{O}, \mathbf{q}+\mathbf{O}, \omega). \quad (15)$$

They can be expressed in terms of the susceptibility matrix χ_0 for noninteracting electrons by means of the equations

$$\begin{aligned} \tilde{\chi}(\mathbf{q}+\mathbf{G}, \mathbf{q}+\mathbf{G}', \omega) &= \chi_0(\mathbf{q}+\mathbf{G}, \mathbf{q}+\mathbf{G}', \omega) + \sum_{\mathbf{G}'', \mathbf{G}'''} \chi_0(\mathbf{q}+\mathbf{G}, \mathbf{q}+\mathbf{G}'', \omega) \\ &\times \frac{\delta V_{\text{xc}}(\mathbf{q}+\mathbf{G}'', \omega)}{\delta n(\mathbf{q}+\mathbf{G}'', \omega)} \tilde{\chi}(\mathbf{q}+\mathbf{G}'', \mathbf{q}+\mathbf{G}', \omega), \end{aligned} \quad (16)$$

$$\begin{aligned} \tilde{\chi}(\mathbf{q}+\mathbf{G}, \mathbf{q}+\mathbf{G}', \omega) &= \tilde{\chi}(\mathbf{q}+\mathbf{G}, \mathbf{q}+\mathbf{G}', \omega) + \sum_{\mathbf{G}''} \tilde{\chi}(\mathbf{q}+\mathbf{G}, \mathbf{q}+\mathbf{G}'', \omega) \\ &\times \frac{4\pi e^2}{|\mathbf{q}+\mathbf{G}''|^2} \tilde{\chi}(\mathbf{q}+\mathbf{G}'', \mathbf{q}+\mathbf{G}', \omega). \end{aligned} \quad (17)$$

We will be interested in the case when $\mathbf{q} \rightarrow 0$, for which the numerical calculations in this paper are carried out. It is readily shown that in the limit as $\mathbf{q} \rightarrow 0$ (more precisely, $q v_F / \omega \rightarrow 0$), the elements of the matrix χ_0 are small of order

$$\begin{aligned} \chi_0(\mathbf{q}+\mathbf{O}, \mathbf{q}+\mathbf{O}, \omega) &\sim O(q^2), \\ \chi_0(\mathbf{q}+\mathbf{O}, \mathbf{q}+\mathbf{G}', \omega) &\sim \chi_0(\mathbf{q}+\mathbf{G}, \mathbf{q}+\mathbf{O}, \omega) \sim O(q), \end{aligned}$$

while the constant

$$\chi_0(\mathbf{q}+\mathbf{G}, \mathbf{q}+\mathbf{G}', \omega)$$

is nonzero. Since

$$\delta V_{\text{xc}}(\mathbf{q}+\mathbf{G}, \omega) / \delta n(\mathbf{q}+\mathbf{G}', \omega) \neq 0$$

for arbitrary \mathbf{G} and \mathbf{G}' , we can rewrite (16) for $\mathbf{q} \rightarrow 0$ as

$$\begin{aligned} \tilde{\chi}(\mathbf{q}+\mathbf{G}, \mathbf{q}+\mathbf{G}', \omega) &= \chi_0(\mathbf{q}+\mathbf{G}, \mathbf{q}+\mathbf{G}', \omega) \\ &+ \sum_{\mathbf{G}'', \mathbf{G}'''} \chi_0(\mathbf{q}+\mathbf{G}, \mathbf{q}+\mathbf{G}'', \omega) \\ &\times \frac{\delta V_{\text{xc}}(\mathbf{q}+\mathbf{G}'', \omega)}{\delta n(\mathbf{q}+\mathbf{G}'', \omega)} \tilde{\chi}(\mathbf{q}+\mathbf{G}'', \mathbf{q}+\mathbf{G}', \omega), \end{aligned} \quad (18)$$

where only terms of lowest order in \mathbf{q} have been retained. The terms in Eq. (17) are of the same order in \mathbf{q} as $\mathbf{q} \rightarrow 0$, and in the long-wave limit we can write

$$\begin{aligned} \tilde{\chi}(\mathbf{q}+\mathbf{G}, \mathbf{q}+\mathbf{G}', \omega) &= \chi_0(\mathbf{q}+\mathbf{G}, \mathbf{q}+\mathbf{G}', \omega) + \sum_{\mathbf{G}'', \mathbf{G}'''} \chi_0(\mathbf{q}+\mathbf{G}, \mathbf{q}+\mathbf{G}'', \omega) \\ &\times \left[\frac{4\pi e^2}{|\mathbf{q}+\mathbf{G}''|^2} \delta_{\mathbf{G}'', \mathbf{G}'''} + \frac{\delta V_{\text{xc}}(\mathbf{q}+\mathbf{G}'', \omega)}{\delta n(\mathbf{q}+\mathbf{G}'', \omega)} \right] \tilde{\chi}(\mathbf{q}+\mathbf{G}'', \mathbf{q}+\mathbf{G}', \omega). \end{aligned} \quad (19)$$

The simplest, most natural way to solve Eq. (19) is by iteration, starting with the approximation $\tilde{\chi} = \chi_0$. The corrections to the zeroth-order solution arise from the fact that \mathbf{G}'' and \mathbf{G}''' are nonzero (these are called the local field corrections). The corrections to the solution $\tilde{\chi} = \chi_0$ in (19) are due to the exchange-correlation interaction and to the shortwave component of the direct Coulomb interaction. The direct Coulomb and the exchange-correlation interactions are known to be comparable in magnitude and decrease as $1/G^2$ as G increases when $\mathbf{G}'' \approx \mathbf{G}''' \approx r_s^{-1}$, where r_s is the mean distance between the electrons. Since these two interactions are of opposite sign, the associated corrections nearly cancel, as was noted in the calculation of $\tilde{\chi}$ for Al carried out in Ref. 16. This suggests that even the lowest-order approximation to the solution of (19) will yield reasonable results, and we will therefore use the approximation

$$\varepsilon_{\text{ex}}(\omega, \mathbf{q}) = 1 - \frac{4\pi e^2}{q^2} \chi_0(\mathbf{q}+\mathbf{O}, \mathbf{q}+\mathbf{O}, \omega) \quad (20)$$

in this paper. It should be noted that the frequently-used random phase approximation neglects effects associated

with the exchange-correlation interaction but fully treats the effects due to the short-wave component ($\mathbf{G} \neq 0$) of the direct Coulomb interaction, and is thus clearly inconsistent.

Expression (20) does not lend itself to explicit calculations in the limit $\mathbf{q} \rightarrow 0$. Using the continuity equation⁴ to transform it in the standard way and explicitly separating out the contribution from intraband transitions ($\lambda = \lambda'$) (Ref. 17), we obtain

$$\varepsilon_m(\omega) = 1 - \frac{\bar{\omega}_p^2}{\omega(\omega + i\delta)} + \frac{8\pi e^2 \hbar^2}{3m^2 \Omega} \times \sum_{\mathbf{k}, \lambda \neq \lambda'} \frac{|\langle \mathbf{k} \lambda' | \hat{\mathbf{p}} | \mathbf{k} \lambda \rangle|^2}{(E_{\mathbf{k}\lambda'} - E_{\mathbf{k}\lambda})^2} \frac{f_{\mathbf{k}\lambda'} - f_{\mathbf{k}\lambda}}{\hbar\omega - E_{\mathbf{k}\lambda'} + E_{\mathbf{k}\lambda} + i\delta} \quad (21)$$

and

$$\bar{\omega}_p^2 = \frac{4\pi e^2 m}{3\Omega} \sum_{\mathbf{k}\lambda} \delta(E_{\mathbf{k}\lambda} - E_F) (\nabla_{\mathbf{k}} E_{\mathbf{k}\lambda})^2 / \hbar^2, \quad (22)$$

where E_F is the Fermi energy. The second and third terms in (21) give the contributions from intra- and interband transitions, respectively.²⁾

Formulas of the type (21) are often used to analyze experimental data and have some properties that will prove to be important below. The Kramers-Kronig formula

$$\varepsilon_m(\omega) = 1 + \frac{2}{\pi} \int_0^{\infty} \frac{d\omega' \omega' \text{Im} \varepsilon_m(\omega')}{\omega'^2 - \omega^2 - i\delta} \quad (23)$$

can be used to express the permittivity $\varepsilon_m(\omega)$ in terms of $\text{Im}\{\varepsilon_m(\omega)\}$, and a similar relation holds for $1/\varepsilon_m(\omega)$ and $\text{Im}\{-1/\varepsilon_m(\omega)\}$. The f -sum rule

$$\frac{m\Omega_0}{2\pi^2 e^2} \int_0^{\infty} d\omega' \omega' \text{Im} \varepsilon_m(\omega') = N, \quad (24)$$

is valid for $\text{Im}\varepsilon_m(\omega)$, where Ω_0 is the volume of an elementary cell containing N electrons, including the electrons in the core. A similar f -sum rule also holds for $\text{Im}\{-1/\varepsilon_m(\omega)\}$. We note that the integration over $\hbar\omega'$ in (24) must extend to very high energies, comparable to the binding energies $\hbar\omega' \sim 10^3 - 10^4$ eV for the deepest levels of the core, and in this situation the f -sum rule is not very useful. In practice, the f -sum rule for finite energies¹⁷ is used much more often:

$$\frac{m\Omega_0}{2\pi^2 e^2} \int_0^{\infty} d\omega' \omega' \text{Im} \varepsilon_m(\omega') = N_{eff}(\omega), \quad (25)$$

$$\frac{m\Omega_0}{2\pi^2 e^2} \int_0^{\infty} d\omega' \omega' \text{Im} \left(-\frac{1}{\varepsilon_m(\omega')} \right) = \tilde{N}_{eff}(\omega). \quad (26)$$

In metals where a wide energy gap $\Delta E_c \approx 50 - 100$ eV separates the valence states from the core states, we can choose $\hbar\omega$ so that

$$\Delta E_v < \hbar\omega < \Delta E_c,$$

where ΔE_v is the energy of the fundamental interband transitions. We then find that

$$N_{eff}(\omega) \approx \tilde{N}_{eff}(\omega) \approx N_v,$$

where N_v is the number of valence electrons in the elementary cell. The above situation occurs in many simple metals, and in this case relations (25) and (26) may be called the f -sum rules for the valence electrons.

However, there are many metals for which considerable overlapping occurs between the energy levels for interband transitions and for transitions from core states, and (25), (26) are then no longer true f -sum rules for the total number of valence electrons for any value of $\hbar\omega$. Instead, they define certain effective values $N_{eff}(\omega)$ and $\tilde{N}_{eff}(\omega)$. Here $N_{eff}(\omega)$ is the number of electrons that participate in optical transitions in the energy interval from 0 to $\hbar\omega$, or equivalently, the sum of the oscillator strengths for the optical transitions. On the other hand, $\tilde{N}_{eff}(\omega)$ determines the intensity of the characteristic energy loss spectrum, or the number of electrons involved in collective density excitations for $0 \leq E \leq \hbar\omega$. By analogy with (25) and (26), we can define N_{eff} and \tilde{N}_{eff} for arbitrary energy intervals, not just $[0, \hbar\omega]$.

II. ELECTRON STRUCTURE OF THE 4d-METALS. CALCULATIONS AND COMPARISON WITH EXPERIMENT

The first step in calculating the characteristic energy loss spectrum is to find the electron band structure of the metal. In this paper we use the LMTO method¹⁸ to calculate the band structure and expand the wave function in spherical harmonics with orbital momentum up to $l_{\max} = 3$. This ensures an error of ~ 0.1 eV within an energy interval ~ 15 eV containing the Fermi surface and an error of ~ 1 eV at 10–25 eV above E_F . We calculated 16 bands altogether, which corresponds to an energy interval of approximately 50 eV. We will show that the loss spectrum is insensitive to the crystal lattice symmetry (assuming equal densities, of course). The results for metals with a close-packed cubic structure (Y, Zr, Tc, Ru) were therefore calculated for an fcc structure with a packing density similar to that for the closely-packed cubic structure; this greatly simplifies the numerical calculations (in addition, the loss spectrum for technetium was also calculated for a bcc structure as a check on the calculations). The self-consistent crystal potentials $V_{eff}(\mathbf{r})$ needed to calculate the band structure from the Schrödinger equation (5) were taken from Ref. 19.

As an illustration we consider the electron structure for niobium, a typical 4d-metal whose state density $N(E)$ is shown in Fig. 1. The Fermi level lies slightly below the center of the 4d band and occupies the energy interval from 6 to 15 eV. The curve $N(E)$ for large E has a very jagged profile that differs markedly from the dependence $N(E)$ postulated in the commonly used s - d model. Analysis of the partial state density curves (Fig. 1) reveals that a strongly hybridized 5p-4f band is present between 21.5 and 50.0 eV. In the lower portion of this band (from 21.5 to 32.5 eV), the p -electrons (more precisely, the states with $l = 1$) give the main contribution to $N(E)$, whereas the f -electrons (states with $l = 3$) give the dominant contribution in the upper portion from 32.5 to 50.0 eV. We will therefore refer to the lower and upper portions of the p - f band as the p - and f -bands, respectively. The valence 5s electrons are concentrated primarily

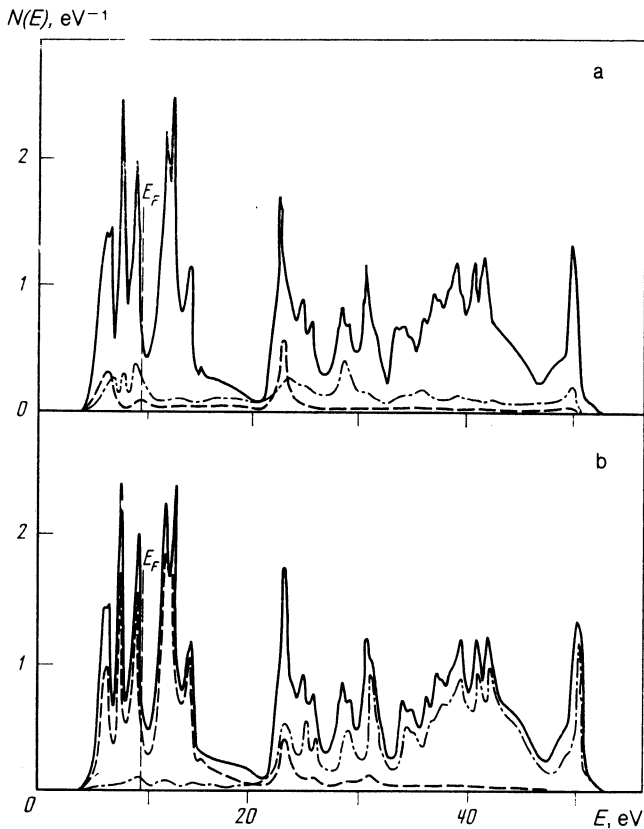


FIG. 1. Total and partial electron state densities in Nb: a) $N_{\text{total}}(E)$ (solid curve), $N_s(E)$ (dashed), $N_p(E)$ (dashed-dotted); b) $N_{\text{total}}(E)$ (solid curve), $N_d(E)$ (dashed), $N_f(E)$ (dashed-dotted).

below the bottom of the $4d$ -band and in its lower portion, as well as in the lower part of the p -band. The electron structure of the $4d$ transition metals has the important feature that $N(E)$ has a pronounced trough which separates the d - and the p -bands, while no such pronounced dip separates the p - and the f -bands. The cutoff of the spectrum at $E \approx 51$ eV is an artifact caused by the small number of basis elements ($l < 3$) used in the electron structure calculations. The shallow depth at which the $4p$ -levels of the core lie (only 35 eV below E_F for niobium) is striking for the $4d$ -metals. Excitation of

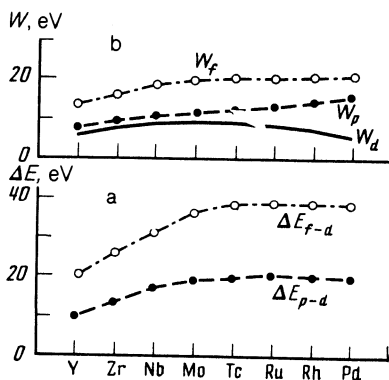


FIG. 2. Band energy difference (a) and band widths (b) for the $4d$ transition metals.

these levels contributes significantly to the optical spectra and to the characteristic energy loss function at high energies. However, this was neglected in our calculations, which therefore inevitably diverge from the experimental values at high energies. Figure 2 shows the width and the relative position of the p -, d -, and f -bands for the other $4d$ -metals.

Once the electron structure of the metal is known, Eqs. (21) and (22) can be used to calculate $\epsilon_m(\omega)$. We first calculated $\text{Im}\epsilon_m(\omega)$ and then used the Kramers-Kronig relations (23) to find $\text{Re}\epsilon_m(\omega)$. The integration in (23) extended up to ~ 50 eV, and the principal-value integrals were calculated accurate to 0.1%. The tetrahedron method^{20,21} was used to perform the integration over the momentum \mathbf{k} . We used 204 points in $1/48$ of the Brillouin zone for the bcc lattice and 175 points for the fcc lattices. The matrix elements $\langle \mathbf{k}\lambda' | \hat{\mathbf{p}} | \mathbf{k}\lambda \rangle$ of the momentum operator were the most difficult to calculate, and the procedure used here was described in detail in Ref. 5. We merely note that the error in calculating $\langle \mathbf{k}\lambda' | \hat{\mathbf{p}} | \mathbf{k}\lambda \rangle$ was 5–10% in a ~ 15 eV interval straddling E_F but increased to 10–30%, 10–25 eV above the Fermi surface and reached 50% or more at still higher energies. This rather large error is due to the variational character of the technique used to solve the Schrödinger equation (5) and to the incompleteness of the system of basis functions used to calculate the band structure. Because of this difficulty, which is common to all numerical methods, $\text{Im}\epsilon_m(\omega)$ is systematically too low, particularly at high energies. A detailed comparison of the experimental data with our calculations of the optical properties of metals [$\text{Im}\epsilon_m(\omega)$ or the conductivity $\sigma(\omega) = (\hbar\omega/4\pi)\text{Im}\epsilon_m(\omega)$] was given previously in Refs. 5 and 6, and we will not discuss these results here. We simply observe that the agreement is not just qualitative but quantitative for most metals.

Figure 3 shows the calculated functions $\text{Im}\{-1/\epsilon_m(\omega)\}$ together with the experimental data on the characteristic energy loss spectra for all of the $4d$ transition metals. The agreement is good, not only in terms of the number and position of the peaks in $\text{Im}\{-1/\epsilon_m(\omega)\}$ but also in terms of the absolute value of the loss function (the results of the optical investigations in Refs. 22 and 23 have been normalized). We briefly mention the principal features of the loss spectra (indicated in Fig. 3 by arrows). The sharp peak at $E_{p1} \approx 10$ eV is present for all of the $4d$ transition metals. This peak is greatly smoothed in the experimental curves and in some cases has the form of a broad, gentle maximum rather than a true peak. The principal peak in the loss spectrum near $E_{p2} \approx 20$ –30 eV is well-defined except for metals at the end of the transition series. In the calculated curves, this peak starts to break up into a series of closely spaced peaks starting at the middle of the transition series, while the experimental curves exhibit an appreciable broadening. At the end of the series, the principal peak splits into two gentle maxima with energies E'_{p2} and E''_{p2} . The maximum at energy E_{pc} is present only on the experimental curves; it is due to excitations of the $4p$ -electrons in the core which were neglected in our calculations and is preceded by a peak at E_{p3} (which on the experimental curves is often a broad, low maximum) which agrees quite well with the cal-

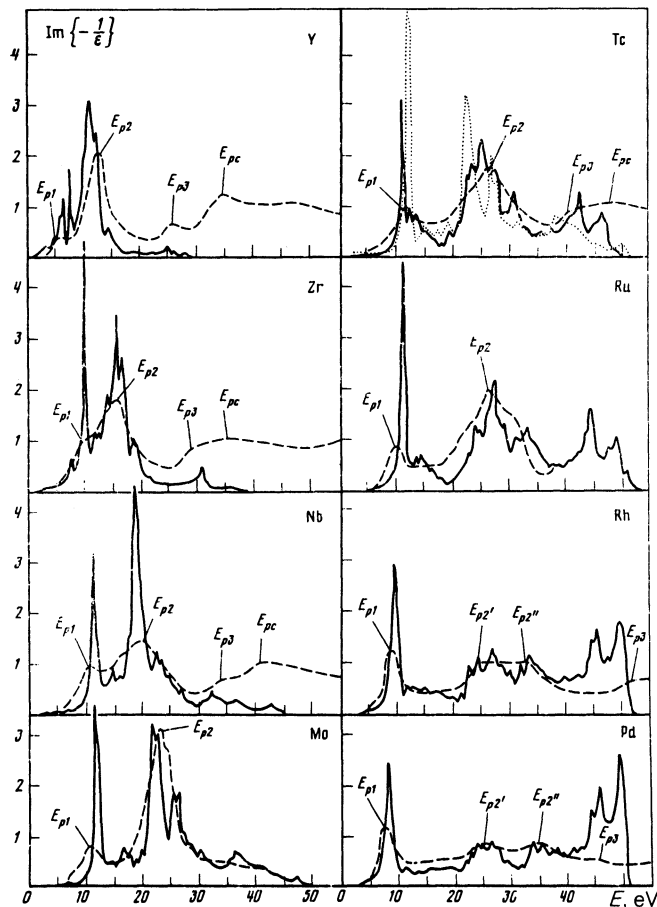


FIG. 3. Characteristic energy loss spectrum for the 4d transition metals; the solid curves show calculated values. Most of the experimental data (dashed curves) are taken from Ref. 1; values from Refs. 22, 24, and 23 are used for Mo, Tc, and Ru, respectively.

culations, although the latter are not very accurate at these energies.

The chief difference between our calculations and the experimental curves is the much greater smoothness of the latter. The smoothness of the curves recorded in Ref. 1 for fast electrons reflected by a surface is hardly surprising, because the characteristic energy loss function averaged over the momentum q was measured there. However, the results in Refs. 24, 22, and 23 were obtained for transmission of fast electrons across a metal film and from light reflection measurements, respectively, i.e., they correspond to zero momentum transfer ($q = 0$), yet even here no fine structure was observed. It was shown in Ref. 25 that this difference cannot be due to the finite resolution of the experimental equipment. Two factors might account for this discrepancy. First, because of the errors in calculating the electron band structure and the matrix elements for the momentum operator, the values of $\text{Im}\epsilon_m(\omega)$ were systematically too low. This is particularly evident for the first peak in the loss spectrum, which for all the 4d-metals occurs at an energy lying in the trough of the $\epsilon_2(\omega)$ curves (or equivalently, $\sigma(\omega)$). If we compare the calculated values of $\sigma(\omega)$ with the experimental data,^{5,6} we find that our values of $\sigma(\omega)$ in the trough

region are considerably lower than the experimental results. This could reflect the fact that in our calculations, the second peak in $\sigma(\omega)$ systematically lies at energies $\sim 0.5\text{--}1$ eV higher than for the experimental data. The second, more important factor that could smooth out the peaks in $\sigma(\omega)$ and $\text{Im}\{-1/\epsilon_m(\omega)\}$ is that the finite lifetimes of the electrons in the excited states may alter the permittivity, and this is completely ignored in the density functional method. The finite lifetime effects are easy to exhibit artificially by averaging the calculated curves $\sigma(\omega)$ over an energy interval whose width increases with $\hbar\omega$. We have not done this, because the result is obvious in any case, and it is easier to use the unsmoothed curve to relate the characteristic energy loss spectrum to the electron structure.

III. ANALYSIS OF LOSS SPECTRA FOR THE 4d TRANSITION METALS

We first examine how the electron transitions determine the structure of the function $\epsilon_m(\omega)$ in the 4d metals. Figure 4 plots the conductivity $\sigma(\omega) = (\hbar\omega/4\pi) \times \text{Im}\epsilon_m^{\text{inter}}(\omega)$ as a function of frequency for the 4d metals. The conductivity directly determines the contribution from each frequency interval to the f -sum rule (25). Table I and Fig. 5 present the numerical data for the principal electron transitions, which we now discuss in more detail.

At low energies $\hbar\omega \lesssim 1$ eV, intraband transitions play the key role. In contrast to the simple metals, however, in the 4d-metals this contribution is by no means dominant in the f -sum rule (25)—it amounts to just 0.6–1.3 electron per atom. The magnitude of the contribution varies irregularly from

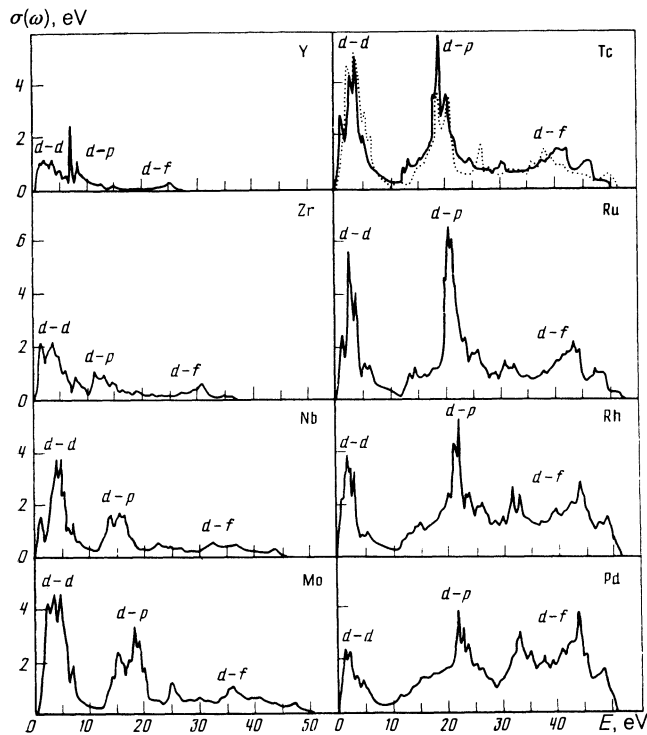


FIG. 4. Calculated interband optical conductivities $\sigma(\omega) = \omega \text{Im}\epsilon(\omega)/4\pi$ for the 4d-metals. The dashed curve for Tc shows results calculated for a bcc lattice.

Metal $\hbar\omega_p$, eV	Calculation					Experiment	
	Transition	E_{trans} , eV	N_{trans}	E_{plasm} , eV	N_{plasm}	E_{plasm} , eV	Feature
Y 11.1	$d-d$	3.1*	1.47	6.5	0.20	4.0	Peak
	$d-p$	7.2	0.29	7.7	0.10	12.4	
		8.5	0.57	11.4	1.95		
Zr 15.4	$d-f$	25.2	0.15	25.2	0.25	25.4	—»—
	$d-d$	3.9*	2.45	10.2	0.48	5.0	Low broad maximum
	$d-p$	11.3	0.38	14.7	0.13	15.8	15.6
16.3		0.21	30.7	0.27	30.7	0.46	28.7
Nb 19.6	$d-d$	4.7*	2.78	11.5	0.48	9.5	Peak
	$d-p$	13.6	0.32	14.5	0.32	19.6	Peak
		15.4	0.48	18.8	1.79		
Mo 23.3	$d-f$	22.5	0.34	22.8	0.91	32.4	Low broad maximum
	$d-d$	32.3	0.37	32.3	0.76	9.9	Peak
		4.8*	2.79	11.8	0.50	14.3	Low broad maximum
Tc 25.9	$d-p$	15.2	0.50	16.5	0.21	22.8	Peak
		18.2	0.78	21.9	1.66	36.0	Low broad maximum
	$d-f$	24.9	0.53	26.1	1.39	11.0	Peak
Ru 28.7	$d-d$	35.9	0.59	36.2	1.36	15.1	Low broad maximum
		4.6*	2.72	11.5	0.29		
	$d-p$	(2.63)	(12.7)	(0.50)		27.0	Peak
12.8		0.10	13.5	0.34			
Rh 29.9	$d-p$	(14.8)	(0.09)	(15.1)	(0.25)	46.0	Low broad maximum
		18.8	1.61	24.0	0.87		
	$d-f$	(18.6)	(1.17)	(23.0)	(1.40)	30.0	Low broad maximum
24.5		0.11	25.4	1.25			
Pd (30.5)	$d-p$	(26.5)	(0.35)	(27.2)	(0.76)	41.1	Very weak, broad maximum.
		30.2	0.35	30.9	1.13		
	$d-f$	(31.1)	(0.30)	(31.6)	(0.65)	49.0	Low broad maximum
37.6		0.43	37.9	0.29			
Zr 15.4	$d-d$	(37.9)	(0.74)	(39.0)	(1.63)	7.9	Peak
		40.2	0.43	42.3			
	$d-p$	45.5	0.29	46.5	0.79	24.6	Broad coalescing maxima
Nb 19.6	$d-d$	(49.4)	(0.14)	(50.0)	(0.22)	32.2	Peak
		4.2*	2.86	11.1	0.35		
	$d-p$	13.9	0.20	14.5	0.31	41.1	Very weak, broad maximum.
20.5		1.63	24.0	0.57	49.0	Low broad maximum	
Mo 23.3	$d-p$	27.2	0.57	27.4	1.17	6.8	Peak
		31.4	0.54	32.0	1.40	16.1	Low broad maximum
	$d-f$	43.3	1.08	44.3	1.78	24.2	Peak
Nb 19.6	$d-d$	47.3	0.31	49.0	1.10	34.3	Peak
		3.8*	1.96	9.8	0.32	46.0	Low broad maximum
	$d-p$	14.8	0.35	15.1	0.34	49.0	Low broad maximum
23.8		2.01	25.8	1.60			
Mo 23.3	$d-p$	32.2	0.93	32.7	1.12	49.0	Low broad maximum
		40.8	1.02	41.2	0.98		
	$d-f$	46.5	0.92	47.6	2.85	6.8	Peak
Nb 19.6	$d-d$	3.0*	1.31	8.3	0.31	16.1	Low broad maximum
		16.2	0.75	17.1	0.34		
	$d-p$	21.8	1.65	24.8	1.10	24.2	Peak
32.8		1.26	34.7	0.83	34.3	Peak	
Mo 23.3	$d-f$	39.0	0.85	39.5	0.84	46.0	Low broad maximum
		43.8	1.03	45.5	2.17		
	$d-d$	47.8	0.47	49.4	1.75		

* The $d-d$ transition energy is taken equal to one-half the width of the d -band; the calculation for Tc was carried out for both fcc and bcc lattices (the latter results are given in parentheses).

one metal to the next in much the same way that $N(E_F)$ does for the metals in the $4d$ -series (Fig. 5).

Transitions between empty and filled subbands of the d -band are dominant at optical energies ($1 \text{ eV} < \hbar\omega \leq 5 \text{ eV}$). Because the momentum operator relates states with $\Delta l = \pm 1$, the matrix elements for the interband $d-d$ transitions can be nonzero only through mixing of states with $l = 1$ and $l = 3$ with the pure d -orbitals—equivalently, in the terminology of the close coupling approximation, through

overlapping of d -orbitals localized at adjacent atoms. However, the large phase volume offsets the small value of the matrix elements for the interband $d-d$ transitions, so that their contribution to the d -sum rule may be larger than for the intraband transitions.

Both types of transition occur within the d -band and have energies $\hbar\omega$ less than $\hbar\omega_p$. It is convenient to combine them into a single group of $d-d$ transitions when analyzing the loss spectra. The contribution from the $d-d$ transitions

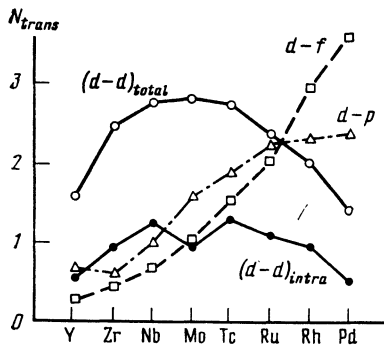


FIG. 5. Oscillator strengths for the principal electron transitions in the 4d metals.

changes regularly along the 4d-series—the contribution is small at the beginning and end of the series, where there are fewer filled (respectively, empty) d -states, and is largest for metals in the middle of the series (Table I and Fig. 5).

The next type of transition to become involved are the transitions from the filled part of the d -band to the unfilled p -band. Because states with $l = 1$ and $l = 3$ dominate in the p -band, the matrix elements for the d - p transitions are several times larger than for the interband d - d transitions. The d - d and d - p transition regions are well-separated for all the 4d-metals (Fig. 4), because the minimum energy required to excite the d - p transitions exceeds the width of the p -band. The d - p transition region is far from homogeneous; $\sigma(\omega)$ has several peaks, with the lowest-energy peak dominating for metals in the beginning and middle of the series, while the maxima at the center and in the upper portion of the d - p transition region dominate for the metals at the end of the series (Ru, Rh, Pd). These peaks are clearly due primarily to the structure of the p -band, which varies appreciably with a characteristic energy scale of 4–7 eV. The energy structure of the d -band has a characteristic scale of 1–2 eV and affects only the fine structure of the d - p transitions [as a typical example we may cite the peaks in $\sigma(\omega)$ at $\hbar\omega = 7.5$ and 8.5 eV for yttrium].

Everything we have said so far concerning the magnitude of the matrix element and the structure of the d - p transitions remains valid for the d - f interband transitions. Because the p - and f -bands are completely free, the total contribution of the d - p and d - f transitions to the f -sum rule increases with the number of d -electrons in the metal (Fig. 5). This dependence is nearly linear except for metals at the start of the series, because the d - p and d - f transition energies increase rapidly as we go from Y to Zr and from Zr to Nb (Fig. 2). The individual N_{d-p} and N_{d-f} contributions for the d - p and d - f transitions do not depend linearly on the atomic number (Fig. 5). This probably reflects the strong interaction between these two groups of transitions due to the high degree of hybridization of the p - and f -bands.

Analysis of the calculated results reveals that the matrix elements for a transition from the bottom of the d -band to the bottom of the p - f band and from the top of the d -band to the top of the p - f band are appreciably larger than for transitions from the bottom (top) of the d -band to the top (bottom) of the p - f band. In terms of chemical bonding,

strong transitions occur either between bonding orbitals, for which the electron density is a maximum at the boundary of the cell, or between antibonding orbitals for which the electron density nearly vanishes at the edge of the cell. Because of this fact, which is associated with the degree of localization of the electron states, the d - p transitions with the lowest energy dominate for the metals at the start and middle of the series, where only the bottom of the d -band is filled. For the metals at the end of the series, the d -band is almost completely filled and the d - p transitions (which now correspond to excitation of electrons from the top of the d -band to the bottom of the p -band) are strongly suppressed. In this case, d - p transitions of higher energy and d - f transitions are most likely to occur.

The above discussion shows that the atomic number of the metal and the width and relative positions of the d -, p - and f -bands are the principal factors determining the primary characteristics of the electron transitions (their energy and contribution to the f -sum rule). The crystal structure influences the fine structure of the band energies but has little influence on these characteristics. Indeed, our calculations for technetium for both bcc and fcc lattices gave very similar results (Table I).

Now that the nature of the principal electron transitions has been determined, we proceed to show how they determine the characteristic energy loss spectrum. We are primarily interested in the low-energy energy loss peak at $\hbar\omega = E_{p1}$ which is present in all the 4d-metals, and in the intense peak at E_{p2} , which is present for all but rhodium and palladium.

The simplest way to understand these peaks is to analyze the real and imaginary parts $\epsilon_1(\omega)$, $\epsilon_2(\omega)$ of the permittivity together. Figure 6 plots calculated values $\epsilon_1(\omega)$ and $\epsilon_2(\omega)$ for Y, Mo, and Pd. We will first discuss the low-energy peak for metals at the beginning and middle of the 4d-series. The curves show that in all cases, $\epsilon_1(\omega)$ changes sign at an energy $\hbar\omega \approx E_{p1}$ lying between the d - d and the d - p transitions. The reason for this behavior is readily understood from the Kramers-Kronig relation if we separate the contributions from the intraband and interband d - d transitions:

$$\epsilon_1(\omega) \approx 1 - \frac{N_{d-d} \omega_p^2}{N_v \omega^2} + \frac{2}{\pi} \int_{E_{p1}/\hbar}^{\infty} \frac{\omega' \epsilon_2(\omega') d\omega'}{\omega'^2 - \omega^2}. \quad (27)$$

Here $\omega_p = (4\pi e^2 N_v / m\Omega)^{1/2}$ is the classical plasma frequency for a homogeneous electron gas of density N_v / Ω , and N_{d-d} is the oscillator strength for the d - d transitions. According to Table I, E_{p1} is less than $\hbar\omega_p (N_{d-d} / N_v)^{1/2}$ for all of the 4d-metals; we would therefore obtain $\epsilon_1(\omega) < 0$ throughout the energy interval between the d - d and d - p transitions if only the contribution from the d - d transitions were considered. The third term in (27) describes the contribution from the d - p transitions, which is positive for $\hbar\omega \approx E_{p1}$ and causes $\epsilon_1(\omega)$ to change sign. Since there are no strong interband transitions at these energies and $\epsilon_2(\omega) \ll 1$, the characteristic energy loss function $\text{Im}\{-1/\epsilon(\omega)\}$ has a sharp peak at an energy E_{p1} which is constrained to lie between the d - d and the d - p transitions. This energy E_{p1} is relatively constant along the 4d-series, as can be seen from Table I. A similar explanation

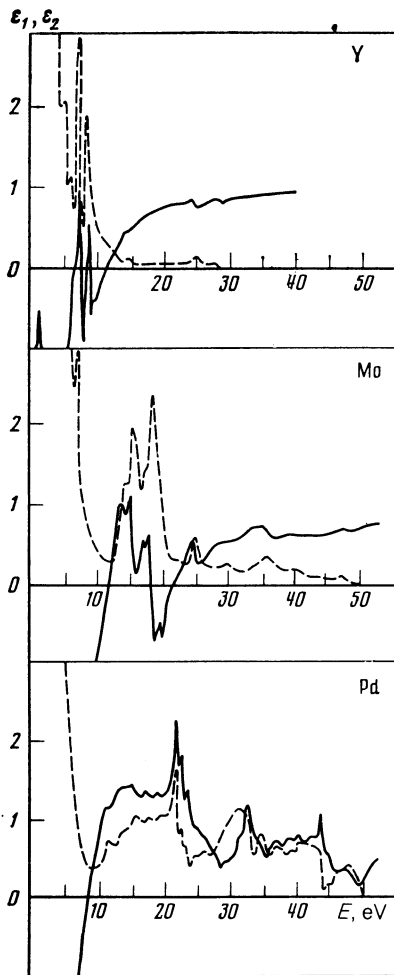


FIG. 6. Permittivity of metals at the beginning (Y), middle (Mo), and end (Pd) of the 4*d*-series; the solid and dashed curves show ϵ_1 and ϵ_2 , respectively.

for the low-energy plasma peak was previously suggested in Ref. 24 on the basis of a phenomenological model allowing for two types of interband transitions with well-separated energies in the transition metals.

Near the intense *d-p* transitions, as ω increases $\epsilon_1(\omega)$ drops sharply to negative values from positive values ~ 1 . This anomalous dispersion is typical for strong interband transitions and is often observed in dielectrics. Since $\epsilon_1(\omega) \rightarrow 1$ as $\omega \rightarrow \infty$, it is clear that $\epsilon_1(\omega)$ must change sign for frequencies lying above the *d-p* transition region. The corresponding energy E_{p2} lies between the *d-p* and the *d-f* transitions at frequencies where $\epsilon_2(\omega) \ll 1$ in these metals (Fig. 6). For metals at the start and middle of the 4*d*-series, the plasma resonance at $\hbar\omega \approx E_{p2}$ is thus a well-defined collective oscillation. More interesting, however, is the fact that E_{p2} lies within 1 eV of $\hbar\omega_p$ for all of the 4*d*-metals at the start and middle of the series. This finding played a key role in previous work, where the plasma resonance was invariably regarded as a plasma oscillation involving all of the conduction electrons. Such an interpretation requires that the energy $\hbar\omega_p$ greatly exceed the energies for all of the principal interband transitions. In this case, we may neglect ω , in favor

of $\omega \sim \omega_p$ in the denominator of the third term in (27) and obtain the simple estimate²⁴

$$E_{p2} \approx \hbar\omega_p (N_{eff}(\omega_p)/N_v)^{1/2}. \quad (28)$$

Since under the above assumptions we also have $N_{eff}(\omega_p) \approx N_v$, we get $E_{p2} \approx \hbar\omega_p$. Actually, however, this analysis is valid only for the simple metals; it represents an oversimplification for the transition metals, in which $\hbar\omega_p$ is comparable to the *d-p* transition energies. Indeed, for the metals from Y to Tc we find that $N_{eff}(\omega_p)$ is just 65–75% of N_v , and the energy E_{p2} estimated by (28) is less than $\hbar\omega_p$ by 14–20% (1.5–5.0 eV). In fact, however, E_{p2} is actually much closer to $\hbar\omega_p$ because the *d-p* transitions lying slightly below E_{p2} contribute more to $\epsilon_1(\omega)$ than is predicted by (28), thereby shifting the plasma resonance toward higher frequencies. It should be noted that both the estimate E_{p2} given by (28) and the energy of the *d-p* transitions that strongly influence the plasma resonance depend on N_v in roughly the same way as $\hbar\omega_p$. This explains why the rough equality $E_{p2} \approx \hbar\omega_p$ holds for all of the 4*d*-metals at the start and middle of the series, even though $\hbar\omega_p$ itself varies by nearly a factor of 2.5. We thus see that in contrast to the simple metals, the near-equality $E_{p2} \approx \hbar\omega_p$ is fortuitous for the transition metals.

At the end of the 4*d*-series (e.g., for Pd), the intense *d-p* transitions occupy a wide energy interval which overlaps the energies for the *d-f* transitions. The anomalous dispersion for these metals extends over the entire interval containing the *d-p* and the *d-f* transitions, and $\epsilon_1(\omega)$ falls off rather slowly without changing sign. All the arguments presented above regarding the plasma resonance at ϵ_{p1} are easily seen to remain valid in this case. However, the plasma oscillation at E_{p2} is not present for Rh and Pd at the end of the 4*d*-series, because $\epsilon_1(\omega) > 0$ for all energies in the *d-p* and *d-f* transition region, while $\epsilon_2(\omega) \sim 1$ (Fig. 6). To be sure, even here $\text{Im}\{-1/\epsilon(\omega)\}$ has weak, very broad maxima at E'_{p2} and E''_{p2} ; this is because the energy distributions of the *d-p* and *d-f* transitions are not completely uniform. However, these maxima are exceptional and depend on the structure of the *p-f* band. An intermediate situation holds for Ru, as one might expect from its position in the periodic table. Although the characteristic energy loss function for Ru has a peak at E_{p2} , it is split by the strong *d-p* and *d-f* transitions and is extremely broad (≈ 10 eV).

The peak at E_{p3} noted in Sec. 2 is intrinsically associated with the *d-f* transitions. It occurs at energies well above $\hbar\omega_p$, for which $\epsilon_2(\omega) \ll 1$ and $\epsilon_1(\omega) \sim 1$ for all the 4*d*-metals (Fig. 6). For these energies

$$\text{Im}\{-1/\epsilon_m(\omega)\} = \epsilon_2(\omega) / (\epsilon_1^2(\omega) + \epsilon_2^2(\omega)) \approx \epsilon_2(\omega),$$

i.e., the peaks in the loss spectrum coincide with the maxima in $\epsilon_2(\omega)$ associated with the *d-f* transitions. Since $\epsilon_1(\omega)$ does not even change sign near these peaks, they would appear to correspond to one-particle excitations rather than to collective plasma oscillations. The actual situation in the 4*d*-metals is more complicated, because electrons are excited from the core 4*p*-level into unoccupied states in the 4*d*-band. As the atomic number *Z* increases, the 4*d*-band fills up and 4*p*-

$4d$ transitions therefore become less likely; however, $4d-4f$ transitions become more likely (Fig. 5, Table I). It remains to determine how these two types of transitions interact.

CONCLUSIONS

Our numerical calculations indicate that the dynamic response functions can be described qualitatively and even quantitatively in a wide frequency range by using the density functional technique to calculate the spectrum of the band electrons. Comparison with experiment shows that the local-field and exchange-correlation effects neglected in our calculations have little influence on the dynamic response. It is unclear whether these effects are individually small or whether they cancel one another. Further work is needed here, as well as to analyze the consequences of the finite lifetime of the excited electrons.

An analysis of the calculated results enabled us to identify the factors responsible for the features of the characteristic energy loss spectra of the transition metals. We have shown that the deep trough in the state density between the d - and p -bands and, to a lesser extent, the nonuniform energy distribution of the electron states above E_F , play a key role. The deep trough in $N(E)$ also explains why the loss spectrum for the transition metals is insensitive to the momentum transfer q (Refs. 2, 24). Our analysis has shown that the relative positions and widths of the p -, d -, and f -bands and the extent to which these bands are filled—i.e., the atomic number Z and the atomic volume—determine the separation of the electron transitions into groups, as well as the energy and the oscillator strength for each group. The crystal structure is of secondary importance and affects only the fine structure of the conductivity $\sigma(\omega)$ and the loss spectrum; this fine structure is almost completely washed out due to the finite lifetime of the excited electrons.

Although we have considered only the $4d$ -metals in this paper, our qualitative results are valid much more generally. Both our calculations and the experimental data indicate that the situation is similar for the $3d$ - and $5d$ -transition metals, and for the noble metals (Cu, Ag, Au) for energies above 10 eV. Compounds of the transition metals are also of great interest here; their electron structures are much more diverse and complex, which is reflected in their more varied characteristic energy loss spectra. We hope that numerical calculations combined with theoretical analysis will lead to progress here in the near future.

In closing, it is a pleasant duty to thank V. L. Ginzburg, L. V. Keldysh, and D. A. Kirzhnitskiĭ for support and valuable discussions. We also thank the participants in seminars

given by V. L. Ginzburg and Yu. M. Kagan for a discussion of this work.

¹Strictly speaking, most of the formulas derived in this section are valid only for the longitudinal permittivity. However, when $q = 0$ the longitudinal and transverse permittivities coincide for cubic crystals, to which we confine ourselves in this paper. We will therefore make no distinction between them.

²The intraband contribution to the permittivity was actually calculated in Refs. 5 and 6 by using the Drude-Zener formula, which unlike (21) treats electron-phonon scattering. However, this makes little difference as far as the characteristic energy loss spectra are concerned.

³M. J. Lynch and J. B. Swan, *Aust. J. Phys.* **21**, 811 (1968).

⁴H. Raether, *Excitations of Plasmon and Interband Transitions by Electrons*, Springer Tracts in Modern Physics, Vol. 88, Springer Verlag, New York, (1980).

⁵K. Sturm, *Adv. Phys.* **31**, 1 (1982).

⁶D. Pines, *Elementary Excitations in Solids*, Benjamin, New York, (1963).

⁷Yu. A. Uspenskii, E. G. Maksimov, S. N. Rashkeev, and I. I. Mazin, *Z. Phys.* **B 53**, 263 (1983).

⁸E. G. Maksimov, I. N. Mazin, S. N. Rashkeev, and Yu. A. Uspenskii, *FIAN Preprint No. 188* (1985).

⁹S. L. Adler, *Phys. Rev.* **126**, 413 (1962).

¹⁰P. Hohenberg and W. Kohn, *Phys. Rev.* **B136**, 864 (1964).

¹¹W. Kohn and L. J. Sham, *Phys. Rev.* **140**, 1130 (1965).

¹²Theory of the Inhomogeneous Electron Gas, S. Lundqvist and N. H. March eds., Plenum Press, New York (1983).

¹³O. V. Dolgov and E. G. Maksimov, *Usp. Fiz. Nauk* **138**, 95 (1981) [*Sov. Phys. Usp.* **25**, 688 (1981)].

¹⁴M. J. Stott and E. Zaremba, *Phys. Rev.* **A21**, 12 (1980).

¹⁵A. Zangwill and P. Sover, *Phys. Rev.* **A21**, 1561 (1970).

¹⁶V. Peukert, *J. Phys.* **C11**, 4945 (1978).

¹⁷W. E. Pickett and C. S. Wang, *Phys. Rev.* **B26**, 4719 (1982).

¹⁸S. P. Singhal, *Phys. Rev.* **B14**, 2352 (1976).

¹⁹D. Y. Smith and E. Shiles, *Phys. Rev.* **B17**, 4683 (1978).

²⁰O. K. Andersen, *Phys. Rev.* **B12**, 3060 (1975).

²¹V. L. Moruzzi, J. F. Janak, and A. R. Williams, *Calculated Electronic Properties of Metals*, Pergamon, New York (1978).

²²G. Lehmann, P. Rennert, M. Taut, and M. Wonn, *Phys. Stat. Sol.* **37**, K27 (1970).

²³O. Jepsen and O. K. Andersen, *Sol. St. Comm.* **9**, 1763 (1971).

²⁴V. M. Maevskii, A. V. Druzhinin, M. M. Kirillova, and L. V. Nomero-vannaya, *Metod Kramersa-Kroniga dlya Opredeleniya Opticheskikh Kharakteristik Metallov v Oblasti Vysokikh Energii* (The Kramers-Kronig Method for Calculating the Optical Properties of Metals at High Energies), VINITI Dep. (1981).

²⁵E. S. Gluskin, A. V. Druzhinin, M. M. Kirillova, et al., *Opt. Spektrosk.* **55**, 891 (1983) [*Opt. Spectrosc. USSR* **55**, 537 (1983)].

²⁶V. D. Gorobchenko, M. V. Zharnikov, E. G. Maksimov, and K. A. Moldasanov, *Zh. Eksp. Teor. Fiz.* **86**, 597 (1984) [*Sov. Phys. JETP* **59**, 348 (1984)].

²⁷M. V. Zharnikov and S. N. Rashkeev, *Fiz. Tverd. Tela* **26**, 3385 (1984) [*Sov. Phys. Solid State* **26**, 2034 (1984)].

Translated by A. Mason